buildings

MDPI

Article

Study of the Freeze–Thaw Resistance for Composite Fiber Recycled Concrete with Sulphate Attack Exposure

Xiaosa Yuan *, Mingjiang Dai, Mengfan Li and Fang Liu

Shaanxi Key Laboratory of Safety and Durability of Concrete Structures, Xijing University, Xi'an 710123, China; 15884130883@163.com (M.D.); limenfan821@163.com (M.L.); liufang_winter@163.com (F.L.)
* Correspondence: yuanxiaosa2009@163.com

Abstract: The exposure of recycled concrete (RCA) to a sulphate environment in cold regions makes it crucial to overcome the freeze–thaw cycling effects of recycled concrete. Based on steel and basalt fiber reinforced recycled concrete, the freeze–thaw cycle resistance of recycled concrete was studied by exposure to a sulphate environment. The mass loss, dynamic elastic modulus loss and compressive strength loss of the specimens were studied through freeze–thaw cycle experiments. SEM techniques were used to explore the effect of fiber distribution on the freeze–thaw resistance of recycled concrete. The freeze–thaw mechanism of the basalt fiber and steel fiber recycled concrete exposed to a sulphate environment has also been summarized. The results show that, based on the sulphate environment, the composite fiber recycled concrete has a higher stability in terms of mass loss and relative dynamic modulus of elasticity than single fiber concrete. The compressive strength of $S_{0.9}$RC (recycled concrete with 0.9% steel fibers) and $BF_{5.5}$RC (recycled concrete containing 5.5 kg/m^3 basalt fibers) increased by 8.62% and 13.62%, respectively, compared to normal recycled concrete after 28 days of maintenance; and after 150 freeze–thaw cycles, the compressive strength increased by 41.39% and 47.54%, respectively; compared to ordinary natural aggregate concrete, the compressive strength of $S_{0.9}$RC and $BF_{5.5}$RC increased by 32.90% and 27.36%, respectively. The compressive strength of the $S_{1.5}BF_{7.5}$RC (recycled concrete with 1.5% steel fibers and 7.5 kg/m^3 basalt fibers) composite basalt fiber–steel fiber concrete also increased by 42.82%. SEM techniques indicated that the basalt fiber in the recycled concrete exhibited fracture damage, which inhibited the development of microcracks within the concrete. When the recycled concrete is subjected to coupled sulphate and freeze–thaw cycles, freezing occurs from the outside in, with ice crystals extending along the cracks into the matrix. Prior to freezing, a negative pressure is created by the compression of the air and the contraction of the salt solution, which pulls the external solution inwards. The brine is in a state where ice and water coexist during the continuous cooling process. The salt solution migrates from the inside to the outside during heating and melting.

Keywords: salt-frost resistance; recycled concrete; steel fiber; basalt fiber; hybrid steel–basalt fiber

check for updates

Citation: Yuan, X.; Dai, M.; Li, M.; Liu, F. Study of the Freeze–Thaw Resistance for Composite Fiber Recycled Concrete with Sulphate Attack Exposure. *Buildings* **2023**, *13*, 1037. https://doi.org/10.3390/buildings13041037

Academic Editor: Ramadhansyah Putra Jaya

Received: 14 March 2023
Revised: 8 April 2023
Accepted: 11 April 2023
Published: 14 April 2023

Copyright: © 2023 by the authors. Licensee MDPI, Basel, Switzerland. This article is an open access article distributed under the terms and conditions of the Creative Commons Attribution (CC BY) license (https://creativecommons.org/licenses/by/4.0/).

1. Introduction

As China's urbanization accelerates, cement, the main building material, is currently consuming resources at an estimated rate of 2.1 billion tons per year. Along with this massive consumption of resources, China's construction waste is growing by hundreds of millions of tons per year. It already accounts for 30~40% of total municipal waste, of which 50~60% is waste concrete. Compared to developed countries such as the US and the UK, the recycling rate of construction waste in China is less than 5% [1]. Therefore, it is necessary to produce recycled concrete from construction waste that can be used in buildings, roads and other facilities in the cold regions of western China in order to conserve resources, improve the urban construction environment and develop a low-carbon and sustainable approach. However, as western China is a seasonally cold region, concrete structures are susceptible to the combined effects of freeze–thaw, salt erosion, carbonation and wind erosion. It is

necessary to research the deterioration mechanism of recycled concrete under the coupled effects of freeze–thaw and salt erosion, and to improve the durability.

At present, a number of studies have been carried out on recycled concrete from different perspectives. Silva et al. point out [2] that there is a partial decrease in the compressive strength of RAC in comparison with that of normal concrete. It was also found that as the rate of RAC replacement increased, compressive strength and modulus of elasticity were decreased [3,4]. Zhenxian [5] concluded that the water–cement ratio was an important factor affecting the elastic modulus of RAC, which increased by 33.7% when the ratio was decreased from 0.8 to 0.4. Amnon and Katz [6] were able to successfully formulate a high strength recycled concrete classified as C60. Alina and Andrze [7] have found that the higher the strength class of the RAC, the faster the corresponding compressive strength is reduced in comparison to that of natural aggregate concrete. Some researchers have discovered that higher strength recycled concrete can be obtained by appropriate selection of constituents and admixtures and by pre-treatment of aggregates [8–12]. Further, the addition of steel fibers can improve the strength and mechanical properties of the recycled concrete and retard the propagation of cracks [13–15]. Some researchers have also reported that basalt fibers can increase the compressive strength and increase the crack resistance of concrete [16,17]. Mahmoud et al. [18–20] demonstrated that both polypropylene fibers and basalt fibers can significantly improve the frost resistance of concrete.

Researchers [8–12] have observed that the shrinkage rate of RAC is 30% to 50% higher than that of ordinary natural aggregate concrete, and Deakins [21] pointed out that the durability factor of RAC is more than 95% at a substitution rate of 100%. As far as impermeability studies are concerned, Hansen and Jin [22,23] showed that the impermeability of RAC is lower than that of natural aggregate concrete and that it decreases as the substitution rate increases. When natural aggregates are replaced by recycled aggregates, the porosity within the concrete will increase, but the percentage increase in porosity will depend on the strength class of the concrete. There have also been various claims that RCA has a rougher surface, which is more adhesive than natural aggregates. Studies have shown that the treatment of recycled aggregate increases the bond strength of the mortar to the aggregate, with the most common treatments being chemical and polymer treatments [12]. When it comes to resistance to salt attack, RCA concrete is almost as resistant to sulphate attack as concrete made from natural aggregates [24,25]. In addition, resistance to sulphate attack can be improved by appropriate use of silica fumes, fly ash, blast-furnace slags and fibrous materials. According to [26,27], the resistance of RCA concrete to alkali-silica reactions is dependent on the source of the recycled concrete aggregates. Researchers have reported that the expansion caused by alkali-silica reaction in recycled concrete can be significantly reduced by the use of low lime fly ash or silica fume [28]. With regard to the resistance to freeze–thaw cycles, many researchers have noted that RCA concrete is sufficiently resistant to freeze–thaw cycles [29–31]. Another study demonstrated this observation [32]. In addition, freeze–thaw resistance is greater in concrete with a higher w/b ratio and higher RCA content. By altering the percentage change in weight, the w/b ratio can be altered to improve freeze–thaw resistance. However, a strong relationship between freeze–thaw loss and concrete can be observed [30,33].

While the above research results are informative for promotion and application of RCA, multi-scale research tools are lacking to study the deterioration mechanism of RCA under the coupled effect of freeze–thaw and salt erosion. In this paper, the recycled aggregates are obtained from the fragments of crushed concrete, and the defects of the recycled concrete are improved by the addition of steel and basalt fibers. The deterioration mechanism of the recycled concrete is revealed through salt freeze–thaw (5% sulphate solution) cycle tests by analyzing macroscopic indicators (mass loss rate, relative dynamic modulus loss and compressive strength change) and microscopic indicators (fiber distribution) in relation to basalt fiber content, steel fiber content and number of freeze–thaw cycles. Theoretical references for the promotion and application of fiber recycled concrete in cold regions can be derived from the research results.

2. Materials and Methods

2.1. Raw Materials

The cement used in the test was P·O 42.5, a type of ordinary Portland cement in Shaanxi Province, China, and first-grade fly ash was applied to this test. The basic properties of both cement and fly ash are shown in Tables 1–4, respectively. The fine aggregate is river sand with a fineness module of 2.83. Table 5 displays the properties of coarse aggregate and recycled aggregate with continuous grading of 4.75–19 mm and fine aggregate. The physical properties of the steel fiber and the basalt fiber are demonstrated in Tables 6 and 7. The water-reducing agent produced by Subote New Materials Co., Ltd. (Nanjing, China) is used as an admixture, whose technical indexes are presented in Table 8. In addition, the properties of anhydrous sodium sulfate produced by Tianjin Zhiyuan Chemical Reagent Co., Ltd. (Tianjin, China) are displayed in Table 9.

Table 1. Chemical composition of cement (%).

SiO_2	Fe_2O_3	Al_2O_3	CaO	MgO	SO_3	Alkali Content	Ignition Loss
22.81	3.36	5.62	61.43	1.35	2.17	0.54	2.60

Table 2. Basic properties of cement.

Density (g/cm^3)	Specific Surface Area (m^2/kg)	Fineness (%)	Setting Time (min)		Compressive Strength (MPa)		Flexural Strength (MPa)	
			Initial	Final	3 d	28 d	3 d	28 d
3.10	360	3.8	125	180	24.0	50.5	4.7	8.3

Table 3. Chemical composition of fly ash (%).

SiO_2	Al_2O_3	Fe_2O_3	CaO	MgO	Na_2O and K_2O
49.02	31.56	6.97	4.88	0.83	1.78

Table 4. Physical properties of fly ash (%).

Fineness (45 μm)	Water Demand Ratio	Ignition Loss	Water Content	SO_3
18	94	3.65	0.3	1.2

Table 5. Physical properties of aggregate.

Type	Apparent Density (kg/cm^3)	Bulk Density (kg/cm^3)	Fineness Modulus/Mx
Fine aggregate	2640	1490	2.83
Coarse aggregate	2840	1730	0.55
Recycled coarse aggregate	2630	1550	4.05

Table 6. Physical properties of steel fiber.

Length (mm)	Diameter (mm)	Tensile Strength (MPa)	Density (g/cm^3)
37	1	400	7.83

Table 7. Physical properties of basalt fiber.

Length (mm)	Diameter (mm)	Thickness (mm)	Density (g/cm^3)	Modulus of Elasticity (GPa)	Tensile Strength (MPa)
18	15	0.5	2.64	110	4800

Table 8. Technical indicators of water-reducing agent.

Appearance	Hydroxyl	pH Value	Moisture	Solubility
White flakes	22~27	5.0~7.0	≤0.5	Soluble in water and a variety of organic substances

Table 9. Physical properties of anhydrous sodium sulfate.

Cl (%)	Ca (%)	PO_4 (%)	N (%)	Fe (%)	K (%)	pH Value	Ignition Loss(%)
≤0.001	≤0.002	≤0.001	≤0.0005	≤0.005	≤0.01	5~8	≤0.2

2.2. Test Method and Process

2.2.1. Rapid Freeze–Thaw Test and Compressive Strength Test

Sodium sulphate was chosen as the solute to be exposed to the sulphate environment and the concentration of the solution was established at 5%. The specimens were soaked in sodium sulphate solution as a corrosive medium for 48 h and then placed in the experimental apparatus for simulation of freeze–thaw cycles in cold western regions. The freeze–thaw cycle time was set at 6 h per cycle and the temperature of the freezing center of the sample was controlled at (−18 ± 2) °C and the thawing temperature was controlled at (5 ± 2) °C. The freeze–thaw cycle and axial compression test setup is shown in Figure 1. The three-dimensional space of the specimen was 100 mm in accordance with GBT50082-2009.

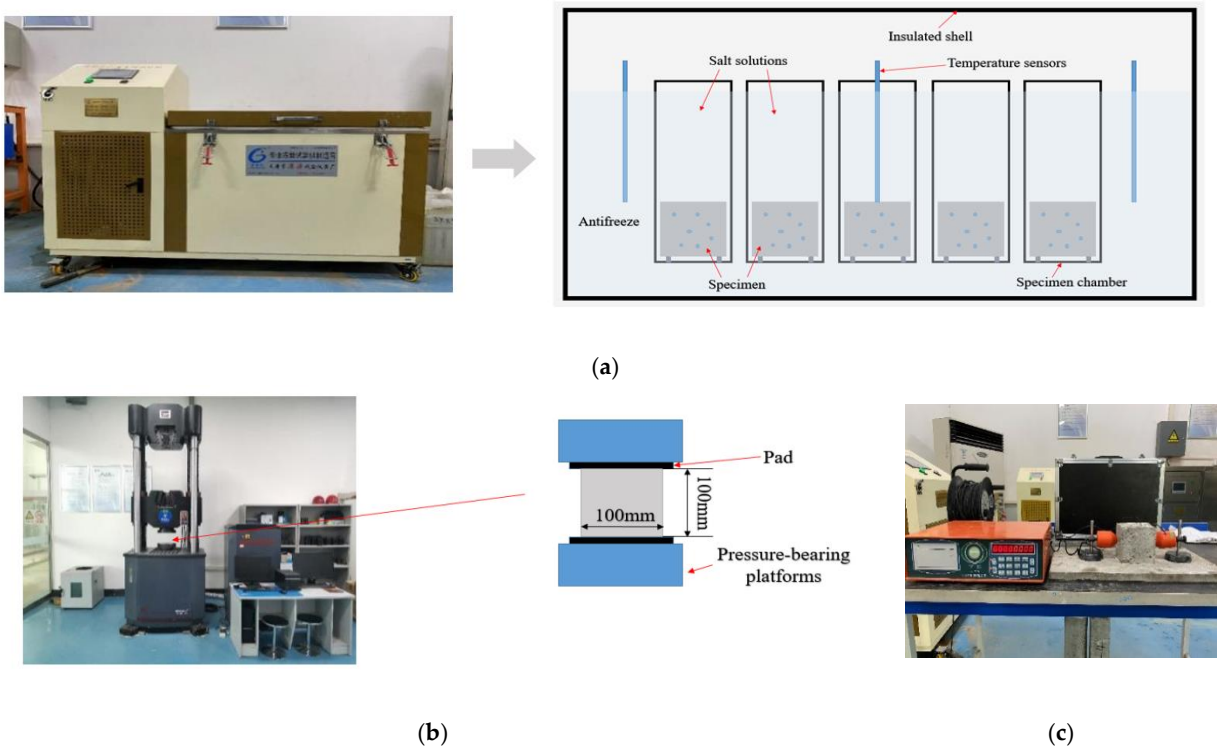


Figure 1. (**a**) Freeze–thaw facility. (**b**) Compressive strength test. (**c**) DT20 dynamic elastometer.

During the freeze–thaw cycle test, the samples are examined over a period of 50 freeze–thaw cycles. The test parameters include specimen mass, specimen dynamic modulus of elasticity and specimen compressive strength. In order for the test data to be reliable, a minimum of 3 specimens are tested for each data and the average value is used as the test value for the relevant index. If the number of freeze–thaw cycles reaches 150, or the rate of mass loss reaches 5%, or the relative dynamic modulus of elasticity decreases by 60%, any of the three conditions is achieved and the test is terminated for that sample. The DT20 dynamic elastometer is demonstrated in Figure 1c. After the sample has reached the required number of freeze–thaw cycles, it is examined on a universal testing machine for axial compressive strength. Prior to the formal application of the load, the instrument applies a pre-stress to the sample to 5 kN, at which point it is checked that the bearing and loading plates at each end of the sample have completed contact with the surface of the specimen, and that the bearing plate, loading plate and center of the specimen are in the same vertical line. The load force is controlled by displacement.

The frost resistance of concrete can be well judged by calculating the mass loss rate 'M_i' and the relative dynamic elastic modulus 'P_i' of the specimens, and the 'M_i' and 'P_i' were based on Formulas (1) and (2).

$$M_i = \frac{G_0 - G_i}{G_0} \times 100\% \quad (1)$$

where, 'M_i' is the mass loss rate at 'i' freeze–thaw cycles, 'G_0' is the initial mass and 'G_i' is the mass at 'i' freeze–thaw cycles.

$$P_i = \frac{f_i^2}{f_{0i}^2} \times 100\% \quad (2)$$

where, 'P_i'is the dynamic elastic modulus at 'i' freeze–thaw cycles, 'f_i' is the fundamental transverse frequency at 'i' freeze–thaw cycles, 'f_{i-1}'is the fundamental transverse frequency at '$i-1$' freeze–thaw cycles.

2.2.2. The Mixed Proportion of Specimens

The mixed properties of the specimens are shown in Table 10. All concrete specimens were de-molded at 24 h after casting and cured in standard curing boxes for 28 days. The NC represents ordinary concrete, and RC is recycled concrete. The $BF_{3.5}RC$ to $BF_{7.5}RC$ are basalt fiber recycled concretes with content from 3.5 to 7.5 kg/m^3. There are steel fiber recycled concretes, including $S_{0.9}RC$, $S_{1.2}RC$ and $S_{1.5}RC$, where S stands for the volume ratio of steel fibers per cubic meter of concrete. Additionally, the specimens from $S_{0.9}BF_{3.5}RC$ to $S_{1.5}BF_{7.5}RC$ represent the steel fiber–basalt fiber recycled concrete (the steel fiber contents from 0.9% to 1.5%, the basalt fiber dosage from 3.5 kg/m^3 to 7.5 kg/m^3).

Table 10. The mixed proportion of specimens.

Type	Cement (kg/m^3)	Water (kg/m^3)	Sand (kg/m^3)	Ordinary Aggregate (kg/m^3)	Recycled Aggregate (kg/m^3)	Water-Reducing Agent (kg/m^3)	S (V%/m^3)	BF (kg/m^3)	Fly Ash (kg/m^3)
NC	347.2	156	708	1061	0	2	0	0	86.8
RC	347.2	156	708	0	1061	2	0	0	86.8
$BF_{3.5}RC$	347.2	156	708	0	1061	2	0	3.5	86.8
$BF_{5.5}RC$	347.2	156	708	0	1061	2	0	5.5	86.8
$BF_{7.5}RC$	347.2	156	708	0	1061	2	0	7.5	86.8
$S_{0.9}RC$	347.2	156	708	0	1061	2	0.9	0	86.8
$S_{1.2}RC$	347.2	156	708	0	1061	2	1.2	0	86.8
$S_{1.5}RC$	347.2	156	708	0	1061	2	1.5	0	86.8

Table 10. *Cont.*

Type	Cement (kg/m^3)	Water (kg/m^3)	Sand (kg/m^3)	Ordinary Aggregate (kg/m^3)	Recycled Aggregate (kg/m^3)	Water-Reducing Agent (kg/m^3)	S (V%/m^3)	BF (kg/m^3)	Fly Ash (kg/m^3)
$S_{0.9}BF_{3.5}RC$	347.2	156	708	0	1061	2	0.9	3.5	86.8
$S_{0.9}BF_{5.5}RC$	347.2	156	708	0	1061	2	0.9	5.5	86.8
$S_{0.9}BF_{7.5}RC$	347.2	156	708	0	1061	2	0.9	7.5	86.8
$S_{1.2}BF_{3.5}RC$	347.2	156	708	0	1061	2	1.2	3.5	86.8
$S_{1.2}BF_{5.5}RC$	347.2	156	708	0	1061	2	1.2	5.5	86.8
$S_{1.2}BF_{7.5}RC$	347.2	156	708	0	1061	2	1.2	7.5	86.8
$S_{1.5}BF_{3.5}RC$	347.2	156	708	0	1061	2	1.5	3.5	86.8
$S_{1.5}BF_{5.5}RC$	347.2	156	708	0	1061	2	1.5	5.5	86.8
$S_{1.5}BF_{7.5}RC$	347.2	156	708	0	1061	2	1.5	7.5	86.8

Note: $S_{0.9}BF_{3.5}RC$ represents 0.9 of steel fiber's content, basalt fiber is dosed at 3.5 kg/m^3, RC stands for recycled aggregate.

3. Results and Discussion

The relative dynamic elastic modulus, mass loss rate and compressive strength loss rate of concrete are the main indicators for judging the concrete damage, and the variation rules of the three indicators are shown in Figures 2–7.

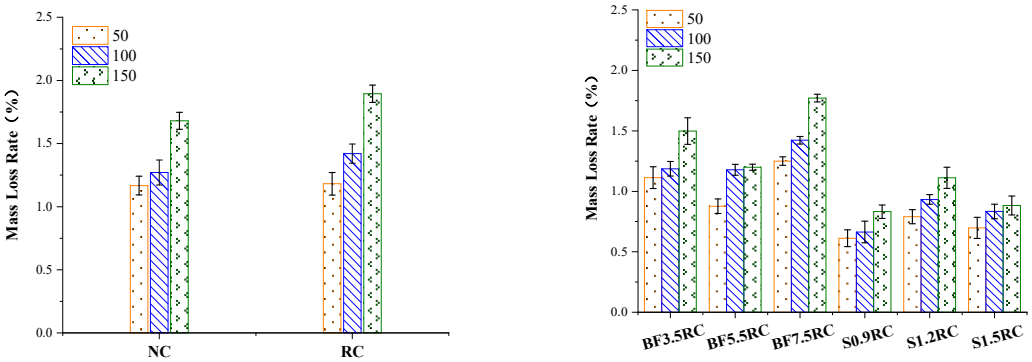


Figure 2. (**a**,**b**) The change in mass loss rate during freeze–thaw cycles. (**a**) NC and RC. (**b**) Steel fiber recycled concrete and basalt fiber recycled concrete.

3.1. Mass Loss Rate

After 50, 100, and 150 freeze–thaw cycles, Figures 2 and 3 show the mass loss rate of the specimens, which are NC, RC, steel fiber recycled concrete and basalt fiber recycled concrete, respectively.

Figure 2 displays the difference in mass loss among ordinary concrete, recycled concrete, single steel fiber recycled concrete and single basalt fiber recycled concrete. Figure 2a demonstrates that the mass loss of ordinary concrete is less than that of recycled concrete during the whole freeze–thaw cycle. During the whole freeze–thaw cycles (50, 100 and 150 freeze–thaw cycles), it can be presented from Figure 2b that the mass loss rate of $S_{0.9}RC$ is the lowest among all single steel fiber recycled concretes, which is 2.11%. Compared with recycled concrete, the accumulated mass loss of $S_{0.9}RC$ during the whole freeze–thaw cycles (50, 100 and 150) decreased by 2.39%. It can be concluded from Figure 2 that the single basalt–steel fiber can decrease the mass loss of recycled concrete to some extent. As can be seen from the figure, the loss of mass of $BF_{5.5}RC$ and BF3.5RC is less than that of BF7.5RC for the recycled concrete with a single basalt fiber. The reason for this may be due to the higher content of basalt fibers in $BF_{7.5}RC$, where there are more exposed parts and more defects on the surface of the specimen than in $BF_{3.5}RC$ and $BF_{5.5}RC$. After 150

freeze–thaw cycles, the mass loss of the specimens is higher because the surface defects are first destroyed by the freeze–thaw action.

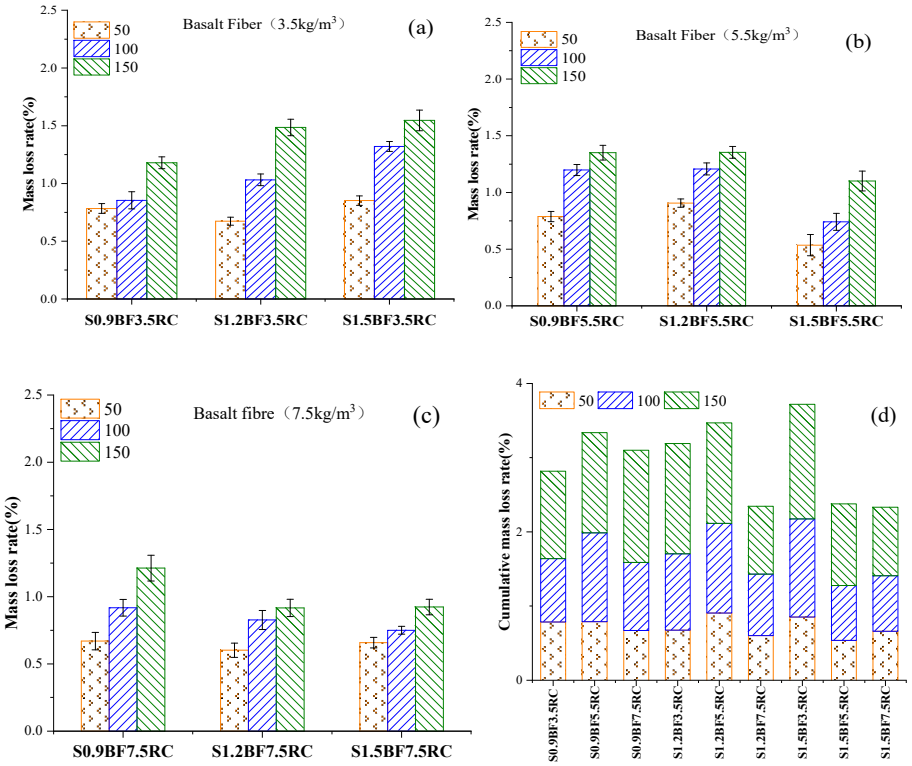


Figure 3. (**a**–**c**) Mass loss rate of steel–basalt fiber recycled concrete. (**d**) The cumulative mass loss rate.

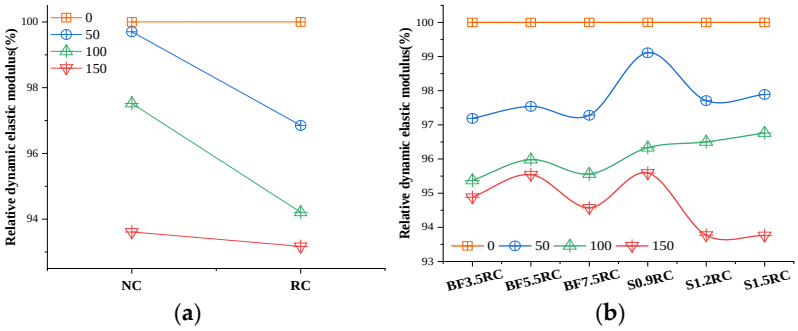


Figure 4. Comparison of relative dynamic elastic modulus. (**a**) NC and RC. (**b**) Fiber-only recycled concrete.

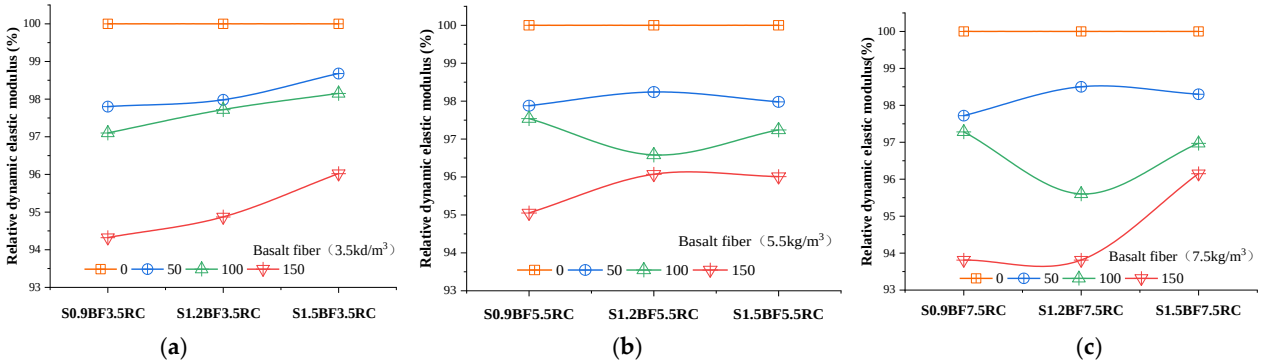


Figure 5. (**a**–**c**) Comparison of relative dynamic elastic modulus.

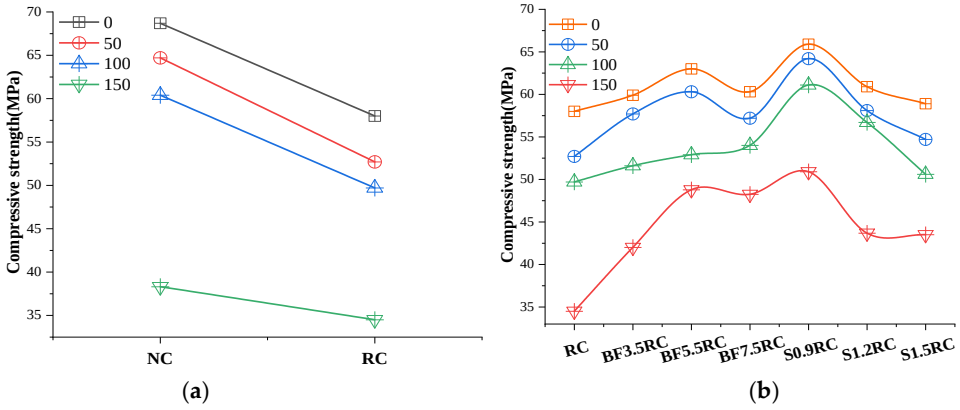


Figure 6. Change in compressive strength during the freeze–thaw period. (**a**) Ordinary and recycled concrete. (**b**) Fiber-only recycled concrete.

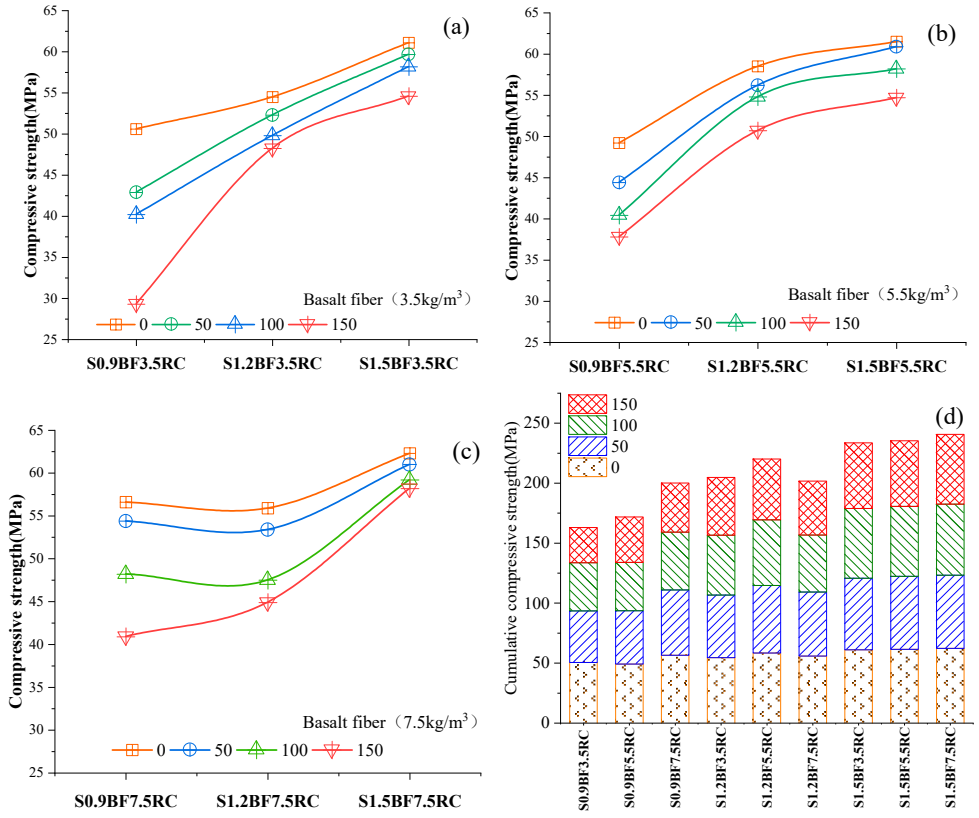


Figure 7. (**a**–**c**) Change in compressive strength during the freeze–thaw period. (**d**) Cumulative cubic compressive strength of the specimen.

Figure 3a–c shows that the mass loss rate increases with the number of freeze–thaw cycles and decreases with increasing fiber amount. Figure 3a shows that the mass loss rate of $S_{0.9}BF_{3.5}$ is lower than that of $S_{1.2}BF_{3.5}RC$, with a cumulative mass loss rate of $S_{0.9}BF_{3.5}RC$ of 2.82%. The cumulative mass loss value of $S_{1.5}BF_{7.5}RC$ is the lowest in all specimens of basalt fiber–steel fiber recycled concrete with 2.33%, as shown in Figure 3d. The main reason may be that steel fiber and basalt fiber make recycled concrete less prone to spalling because fiber can increase internal stress and prevent the expansion of cracks [34].

3.2. Relative Dynamic Modulus of Elasticity

During the whole freeze–thaw cycle, a comparison of the relative dynamic elastic modulus from NC to $S_{1.5}RC$ is shown in Figure 4.

It can be seen from Figure 4a that the relative dynamic elastic modulus of recycled concrete decreases significantly during the freeze–thaw cycle. As the number of freeze–thaw cycles increases, the relative dynamic elastic moduli of all the specimens mentioned above decrease significantly, as shown in Figure 4. The smallest relative dynamic elastic modulus loss is $S_{0.9}$RC at 150 freeze–thaw cycles in the series of fiber-only recycled concrete. Compared with RC, the relative dynamic modulus of $S_{0.9}$RC increases by 2.42%. This result indicates that adding fiber to recycled concrete improves the dynamic elastic modulus to some extent.

The relative dynamic modulus of $S_{1.5}BF_{3.5}$RC is higher than other specimens at 150 freeze–thaw cycles, as shown in Figure 5a. Compared with $S_{1.5}BF_{3.5}$RC, the relative dynamic elastic modulus of $S_{1.5}BF_{5.5}$RC increased by 0.01% seen in Figure 5b, while the $S_{1.5}BF_{7.5}$RC increased by 0.14% displayed in Figure 5c. It is concluded that the specimen of $S_{1.5}BF_{7.5}$RC has good compactness. The relative dynamic elastic modulus of all the specimens decreases during the whole freeze–thaw cycle due to the sulfate attack phenomenon and expansion stress inside the test block. On the one hand, appropriate amounts of steel fibers and basalt fibers can effectively inhibit the generation and development of concrete microcracks; on the other hand, it can refine the coarse pore structure, reduce the total porosity and harmful porosity, and improve the bonding ability of the aggregate and the cement matrix [35,36].

3.3. Compressive Strength of Concrete Mixed with Steel Fiber and Basalt Fiber

The compressive strength of specimens is displayed in Figures 6 and 7.

Figure 6 shows that the compressive strength of the specimens decreases with the increase in freeze–thaw cycles. It can be seen from Figure 6a that the compressive strength of RC is lower than that of NC during the whole freeze–thaw cycle. The compressive strength of $S_{0.9}$RC is higher than that of other specimens at the same freeze–thaw cycle, which is 65.9 MPa, 64.2 MPa, 61.1 MPa, and 50.9 MPa, respectively, as shown in Figure 6b. The reason may be that the steel fiber mainly played an essential role in enhancing compressive strength [37]. Nevertheless, appropriate steel fiber proportion contributes to the compressive strength of recycled concrete, while excess steel fiber weakens it. It can be seen from Figure 6b that the compressive strength of $S_{1.5}$RC decreases with more steel than $S_{0.9}$RC and $S_{1.2}$RC. The excessive content of steel fibers, which tend to cause agglomeration, may be the reason for this phenomenon.

$S_{1.5}BF_{3.5}$RC has a higher compressive strength than $S_{0.9}BF_{3.5}$RC and $S_{1.2}BF_{3.5}$RC at 150 freeze–thaw cycles, as shown in Figure 7a. Compared with $S_{1.5}BF_{3.5}$RC, the compressive strength of $S_{1.5}BF_{5.5}$RC increases by 0.65%, 2.04%, 0.05%, and 0.18%, respectively, while the $S_{1.5}BF_{7.5}$RC improves by 1.96%, 2.21%, 1.77% and 6.59%, respectively, as demonstrated in Figure 7c. It can be seen from Figure 7d that the highest cumulative compressive strength is $S_{1.5}BF_{7.5}$RC up to 240.7MPa. The main reasons may be the internal pore structure improved by the incorporation of steel fiber and basalt fiber and the bonding force between the fiber and the matrix. Compared with the compressive strength of $S_{0.9}$RC, it can be found that the overall compressive strength of $S_{1.5}BF_{7.5}$RC is better. The main reason may be that the toughness under compression increases with fiber content [38–40].

Figure 8 demonstrates the change in compressive strength rate during the freeze–thaw cycle. The compressive strength loss rate creases at 150 freeze–thaw cycles, displayed in Figure 8a, which shows that the anti-freezing ability drops sharply at this time. It can be seen from Figure 8b that the compressive strength loss rate of the specimens added with fibers decreased to varying degrees at 150 freeze–thaw cycles. Compared with the RC compressive strength loss rate of 20.52%, $BF_{7.5}$RC is 20.00%, which is the smallest compressive strength loss rate among all specimens.

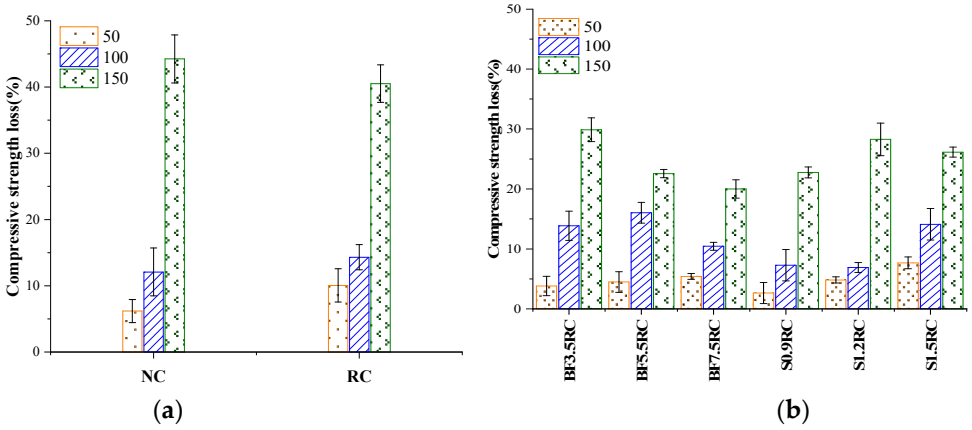


Figure 8. Change in compressive strength rate during the freeze–thaw cycle. (**a**) NC and RC. (**b**) Fiber-only recycled concrete.

It can be seen from Figure 9 that the compressive strength loss rate decreases as the dosage of basalt fiber and steel fiber increases. When the BF content is 3.5 kg/m^3 (Figure 9a), the compressive strength loss rate of $S_{1.5}BF_{3.5}RC$ decreased by 6.82%, 9.51%, and 29.88% compared to RC during whole freeze–thaw cycles (50, 100 and 150 freeze–thaw cycles). As the BF content increases to 5.5 kg/m^3 (Figure 9b), the strength loss rate value of $S_{1.5}BF_{5.5}RC$ is reduced. When the BF content is 7.5 kg/m^3 (Figure 9c), the $S_{1.5}BF_{7.5}RC$ is the same as $S_{1.5}BF_{5.5}RC$. The reason may be that the addition of basalt fiber can improve the bonding force between the steel fiber and the recycled aggregate, which makes the aggregate unseparated from the cement base. Moreover, the hybrid fiber can lower the expansion stress generated inside the concrete, improve the integrity of the concrete, and reduce the loss of strength [13,41,42].

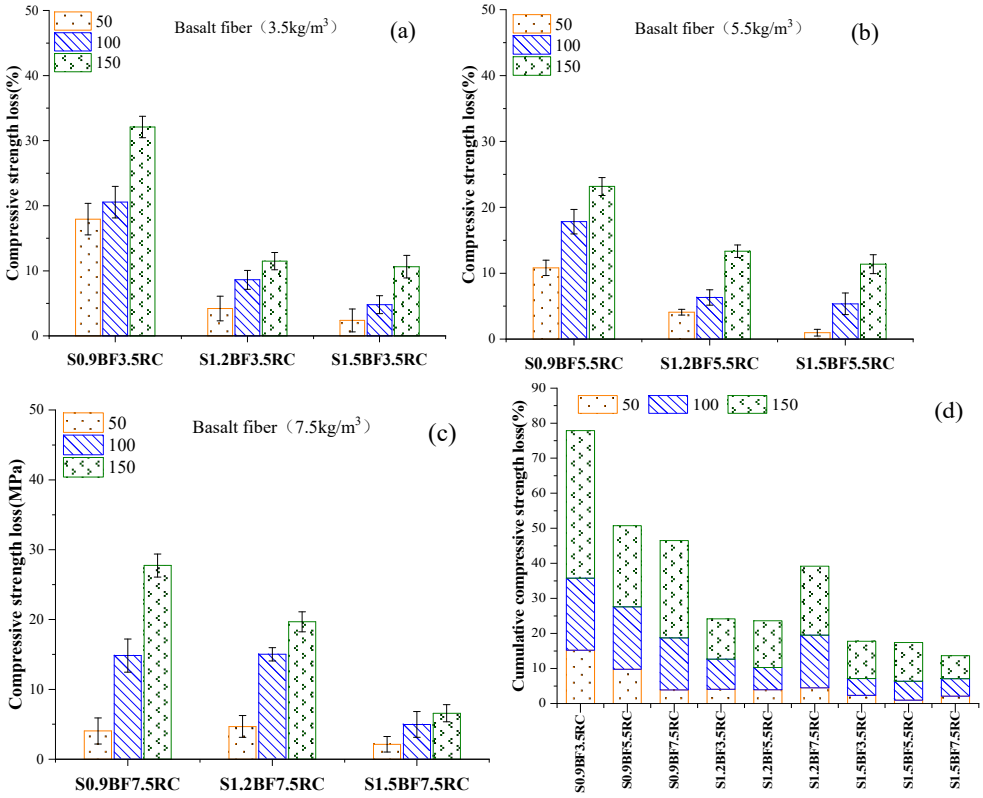
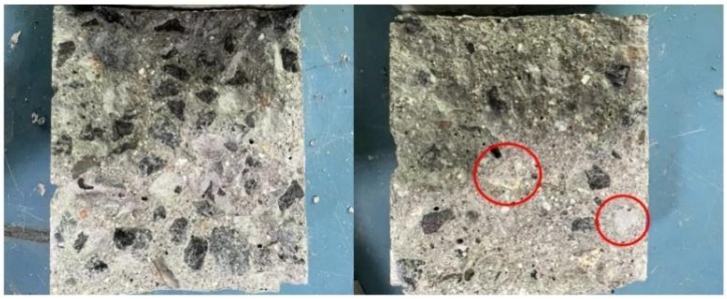


Figure 9. (**a**–**c**) Change in compressive strength rate during the freeze–thaw period. (**d**) Cumulative cubic compressive strength rate of the specimen.

3.4. Detailed Analysis

Figure 10 illustrates how the internal structure of NC and RC concrete behaves. It can be visualized from the figures that there are more NC visible aggregates than RC. This may be due to the fact that the recycled aggregate was obtained from laboratory high-strength concrete that had been mechanically crushed. The mechanical crushing process transforms the concrete from large pieces into smaller pieces with a large number of hairline fractures at the edges of the smaller pieces. Their addition to the concrete, based on the coupling of freeze–thaw cycles and sulphate, makes the concrete matrix in the RC less monolithic and eventually causes a dramatic decrease in the compressive strength of the concrete.



(**a**) (**b**)

Figure 10. Internal structural morphology of NC and RC concrete. (**a**) NC. (**b**) RC.

Figure 11 demonstrates the internal structure of the single admixture concrete. From Figure 11a, it can be seen that the single admixture BF does not visualize its corresponding classified structural situation so it was specifically analyzed in the subsequent SEM experiments. As can be seen in Figure 11b, at this point, the S content is lower and therefore more loosely distributed and less prone to agglomeration. The macroscopic data reveal that the overall frost resistance of the concrete decreases as the S content of the single admixture increases, probably because the single admixture of steel fibers is not suitable for uniform dispersion during the mixing process of production, and increasing its admixture equates to increasing its weakness. This phenomenon indicates that steel fibers have some synergistic effect with basalt fibers.



(**a**) (**b**)

Figure 11. Structural internal morphology of RC concrete with BF and S alone. (**a**) $BF_{5.5}RC$. (**b**) $S_{0.9}RC$.

Figure 12 revealed the manifestation pattern of the internal structure of S–BF–RC concrete. It can be visually seen from the figure that the S distribution is more loosely distributed and agglomeration improves significantly with increasing BF admixture under constant S admixture conditions. The reason for this is probably due to the nature of the steel fibers themselves, which makes it possible to effectively increase the compressive strength of the recycled concrete and the fact that the steel fibers are therefore not so easily dispersed evenly during the concrete mixing process. The addition of basalt fibers makes it easier to disperse the fibers evenly during the mixing process due to the different nature of the two fibers, decreasing the formation of agglomerates. This counteracts the expansion

of the ice crystals during the freeze–thaw cycle, as well as the increased support of the concrete by the steel fibers during the compressive process; the basalt fibers improve its toughness and the two fibers themselves are independent of the freeze–thaw environment, thus together boosting the compressive strength of the recycled concrete.



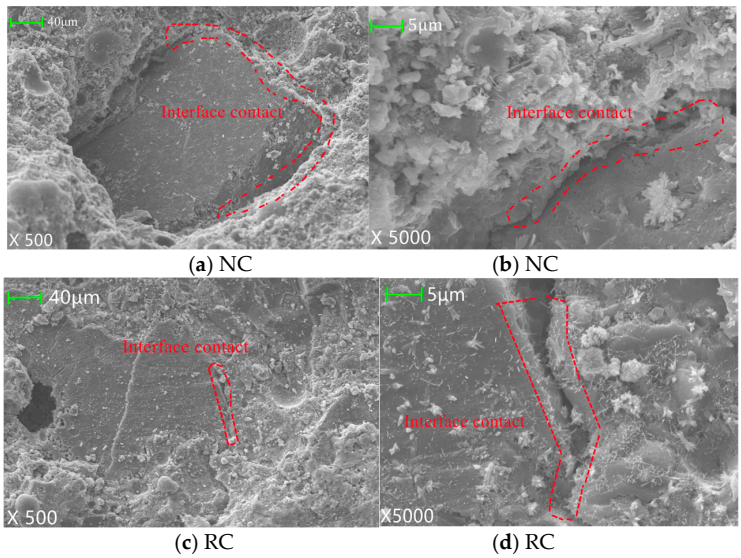
(**a**) (**b**) (**c**)

Figure 12. Structural internal morphology of S–BF–RC concrete. (**a**) $S_{1.5}BF_{3.5}RC$. (**b**) $S_{1.5}BF_{5.5}RC$. (**c**) $S_{1.5}BF_{7.5}RC$.

3.5. Microanalysis

(1) From the above, it can be concluded that the compressive strength of recycled concrete is lower than that of ordinary concrete under different numbers of freeze–thaw cycles. In order to better analyze the reasons for strength loss, the micro-level factors were further explored by scanning electron microscopy.

Figure 13 presents SEM images of ordinary concrete and recycled concrete at the end of a 28 d curing. As can be seen from Figure 13, ordinary concrete, under the condition of not experiencing freeze–thaw cycles, has a strong bond between the cement paste and the aggregate, with structural integrity and good state of hydration products, as shown in Figure 13a,b. However, the recycled concrete, under the same conditions, has relatively loose bonds between the cement paste and the recycled aggregate and the structure is not sufficiently complete, as illustrated in Figure 13c,d. By comparing Figure 13a with Figure 13c, it is evident that without freeze–thaw cycles, the recycled aggregate has developed fine cracks, which are not penetrated and have a lesser effect on the compressive strength. Under the action of freeze–thaw cycles, the original cracks within the concrete become continuously larger as a result of the expansion force of the ice crystals, thus causing the internal structure of the concrete to be destroyed. For this reason, the compressive strength gradually decreases as the number of freeze–thaw cycles increases.



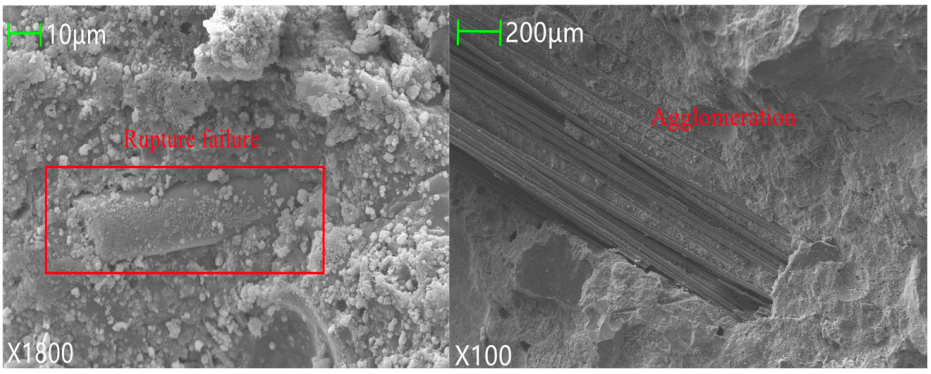
(**a**) NC (**b**) NC

(**c**) RC (**d**) RC

Figure 13. SEM image of NC and RC concrete.

(2) The macroscopic data analysis indicated that the basalt fibers optimized the compressive strength of the recycled concrete under different numbers of freeze–thaw cycles, among which BF7.5 had the most significant effect. To better explain the reasons for this, the micro-level factors were further explored by SEM methods.

Figure 14 presents SEM images of concrete with a BF dosage of 5.5 kg/m^3 under 0 freeze–thaw cycles. It can be seen from Figure 14a that the basalt fibers are fracture damaged in compression, rather than pull-out damage. This means that basalt fibers act as a barrier to the expansion of microcracks within the matrix and a deterrent to the occurrence and development of macro-cracks through molecular adsorption between the surface of the cement paste and the cementitious forces between the matrix. Therefore, increasing the dosage of BF can increase compressive strength. Figure 14a demonstrates that the fibers are mostly concentrated in one direction within the concrete matrix with low fiber spacing and low dispersion. When the BF admixture is increased to 7.5 kg/m^3, the excessive fibers incorporated into the concrete increase the chance of fiber overlap, agglomeration and overlap, increasing the number of weak links within the concrete. This may consequently lead to a significant decrease in the mechanical properties of the concrete, as shown in Figure 14b.



(**a**) (**b**)

Figure 14. SEM image of $BF_{5.5}RC$ and $BF_{7.5}RC$ concrete. (**a**) $BF_{5.5}RC$. (**b**) $BF_{7.5}RC$.

3.6. Salt-Freeze Coupling Mechanism

Freeze–thaw deterioration of S–BF composite fiber recycled concrete based on a sulphate environment is shown in Figure 15. In this paper, the deterioration is divided into pre-freeze, continuous freezing phase and thawing phase.

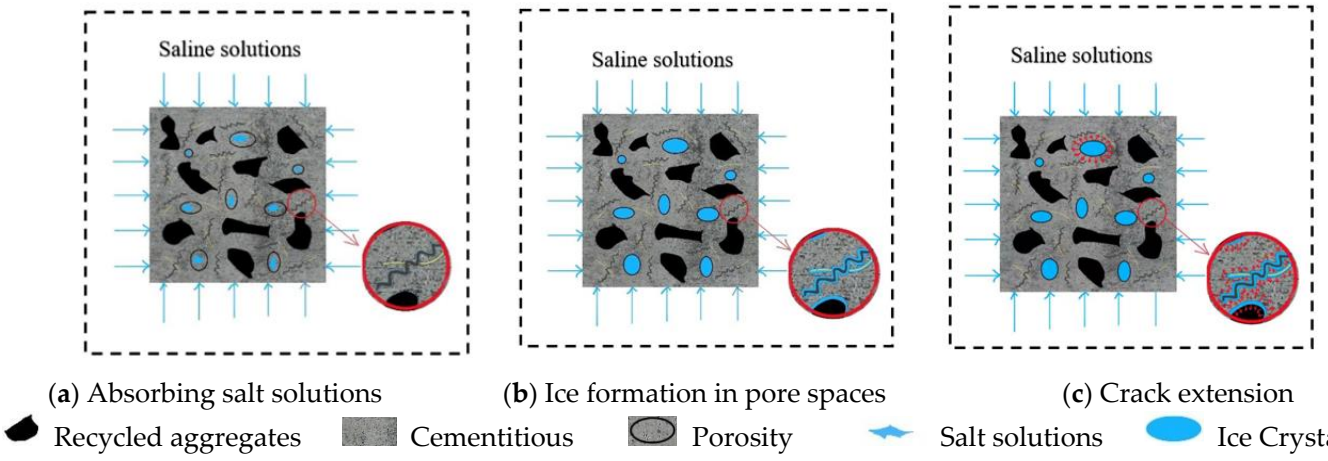


Figure 15. Deterioration phenomenon with S–BF recycled concrete.

Pre-freeze. The concrete is in a sulphate environment. The sulphate solution under the dual action of osmotic pressure and freezing force slowly started to penetrate from the microcracks and linked capillary pores of the concrete to the interior concrete, as shown in Figure 15a. At the same time, the sulphate solution also started to move from the connected capillary pores to the interior of the concrete. This causes the sulphate solution within the microcracks to move more rapidly as the air in the pores inside the concrete contracts at the onset of freezing until the microcracks and capillary pore channels in the concrete are filled with the salt solution. The rate of penetration for the sulphate solution was related to the complexity of the distribution pores and microcracks within the concrete. The sulphate lowers the ice point of water, which also increased the time for the sulphate to move into the concrete interior. During the movement of sulphate toward the interior of the concrete, sulphate ions interact with cement hydration products in the microcracks or capillary pores to produce expansive substances, such as gypsum and calcium alumina. The more sulphate solution there was, the more saturated the solution was in the microcracks and capillary pores, and the more expansive substance content was generated.

Continuous frozen stage. At this stage, the sulphate solution had reached its frozen point. Since the test equipment simulated the freeze–thaw environment in the western cold region, the frozen phenomenon was carried out from the outside to the inside, so the capillary pores and microcracks on the concrete surface would freeze first, and then the ice crystals gradually grew the capillary pores and microcracks inside, and also blocked the passage for the sulphate solution to proceed inside the concrete. At this point, the concrete interior was coexisting with the sulphate solution, air and ice crystals, as shown in Figure 15b. As a result of the freeze concentration principle, part of the water in the sulphate solution was frozen, which caused the sulphate solution concentration to reach saturation after the sulphate was precipitated and attached to the crack or pore wall. The existence of freezing stresses between the ice crystals and the solution would force the sulphate solution to move continuously towards the interior of the concrete until the sulphate solution was completely frozen under the effect of the temperature field. The frozen phenomenon leads to an increase in the volume of the ice crystals, which generates freezing stresses on the microcracks or pore walls, further extending the microcracks. The pores generate high internal stresses due to the continued generation of swellings and salt resulting in cracks within the concrete and accelerated expansion over time, illustrated in Figure 15c. However, some of the freezing and swelling stresses were transferred to the fibers because of the presence of steel and basalt fibers in the recycled concrete.

The melt stage. During this stage, the temperature in the pores or cracks was lower than the surface of the concrete and melting proceeded from the surface ice crystals to the interior. As ice crystals in the pores or microcracks on the surface of the concrete melt, the internal pores keep the solution moving outwards as there is freezing stress; the melting temperature rises until the ice crystals completely dissolve and the solution would continue to move outwards, migrating swelling materials such as gypsum and calcium alumina in the process.

In summary, the mechanism of freeze–thaw deterioration of the specimens when the recycled concrete is exposed to sulphate was as follows. Firstly, the sulphate reduced the icing point of the water and increased the time for the sulphate solution to enter the interior of the recycled concrete. It also increased the content of sulphate solution inside the recycled concrete. Secondly, the expansion stresses generated by the expansive material generated in the sulphate solution entering the recycled concrete are weakened by the presence of steel and basalt fibers. The freeze stresses generated due to the decreased ice point were also weakened by the presence of the fibers. Finally, the stresses on the pore walls or cracks resulting from the continuous precipitation of sulphate during the migration of the sulphate solution adhering to the pore wall or crack interface were also weakened by the fibers.

4. Conclusions

In a sulphate attack environment, the incorporation of basalt and steel fibers into recycled concrete has a significant improvement on the expansion of internal pores and cracks. Additionally, the following results displayed in this paper may be limited to the specimens used in this research.

(1) Throughout the freeze–thaw cycle, cumulative spalling of BF5.5 was 3.25% and compared to natural aggregate concrete, compressive strength was increased by 27.36% for BF5.5RC and 32.90% for S0.9RC. The relative dynamic modulus of elasticity of S0.9RC was increased by 1.98%. The test results indicate that the poor freeze resistance of the recycled concrete exposed to the sulphate environment can be compensated for by the basalt and steel fibers. After 150 freeze–thaw cycles, the compressive strength of the S1.5BF7.5RC composite fibers was increased by 42.80% and the cumulative loss of mass was reduced by 43.39% in comparison with the ordinary concrete. Incorporating basalt fibers and steel fibers together in recycled concrete can increase basalt fiber incorporation and decrease fiber agglomeration.

(2) In a freeze–thaw cycle, the sulfate solution attacks the recycled concrete by freezing from the outside to the inside, the ice crystals extend along the cracks to the inside of the matrix, and the pore wall pressure contributes to the expansion and development of the cracks. Air and brine in the pores contract during freezing, creating a negative pressure that attracts external brine inwards. As the concrete continues to cool, ice crystals and unfrozen solution coexist. When the salt solution heats up and melts, the residual freezing pressure and the temperature difference between the inside and outside forces it to move outwards. The sulphate lowers the freezing point of the concrete and the diffusion behavior of the sulphate ions, resulting in increased liquid uptake by the concrete and an excess of aqueous solution that exacerbates the freeze–thaw damage. Concrete freezes in layers due to the high external and low internal concentration of the salt solution.

(3) In composite fiber recycled concrete, the expansion stresses generated by the sulphate solution during migration are also weakened due to the presence of steel and basalt fibers; the freezing stresses generated by the reduced freezing point of the salt solution are also weakened by the presence of the fibers; and the stresses on the pore wall or fracture are also weakened by the presence of the fibers. Such stresses are generated by the continuous precipitation of sulphate from the sulphate solution as it migrates and thus adheres to the pore wall or fracture interface.

Author Contributions: Methodology and investigation, X.Y.; Original draft preparation, M.D.; Resources and writing, M.L.; Review, editing, and supervision, F.L. All authors have read and agreed to the published version of the manuscript.

Funding: This study is sponsored by the Key Scientific Research Project of Shaanxi Provincial Department of Education (no. 22JS042), the Fundamental Research Fund of Xijing University (no. XJ19B04), the Fund of Education Department of Shaanxi Province (no. 19JK0911), and the Youth Innovation Team Research Project of Shaanxi Provincial Department of Education (no. 22JP099 and 21JP137).

Data Availability Statement: Some or all data, models, or code that support the findings of this study are available from the corresponding author upon reasonable request.

Conflicts of Interest: The authors declare no conflict of interest.

References

1. Xuesheng, Z.; Shuyou, Z.; Delei, S. Scientifically constructing a closed-chain management system for construction waste: An introduction to Beijing's construction waste management experience. *Urban Manag. Technol.* **2018**, *20*, 4447. (In Chinese)
2. Silva, R.V.; Brito, J.D.; Dhir, R.K. Establishing a relationship between modulus of elasticity and compressive strength of recycled aggregate concrete. *J. Clean. Prod.* **2016**, *112*, 2171–2186. [CrossRef]
3. Li, Y.; Fu, T.; Wang, R.; Li, Y. An assessment of microcracks in the interfacial transition zone of recycled concrete aggregates cured by CO_2. *Constr. Build. Mater.* **2020**, *236*, 117543. [CrossRef]

4. Li, L.; Poon, C.S.; Xiao, J.; Xuan, D. Effect of carbonated recycled coarse aggregate on the dynamic compressive behavior of recycled aggregate concrete. *Constr. Build. Mater.* **2017**, *151*, 52–62. [CrossRef]
5. Zhenxian, Z.; Yuenong, Z. Research on the basic properties of recycled concrete. *J. North China Inst. Water Resour. Hydropower* **2012**, *19*, 30–32. (In Chinese)
6. Katz, A. Treatments for the Improvement of Recycled Aggregate. *J. Mater. Civ. Eng.* **2014**, *16*, 597–603. [CrossRef]
7. Andrze, A.; Alina, K. Influence of Recycled Aggregate on Mechanical Properties of HS/HPC. *Cem. Concr. Compos.* **2012**, *24*, 269–279.
8. Zhang, J.; Zhang, F. Pre-treatment of recycled aggregates affected to mechanics performances of concrete. *Mine Constr. Technol.* **2018**, *39*, 20–24. (In Chinese)
9. Zhao, Z.; Wang, S.; Lu, L.; Gong, C. Evaluation of pre-coated recycled aggregate for concrete and mortar. *Constr. Build. Mater.* **2013**, *43*, 191–196. [CrossRef]
10. Zhan, M.; Pan, G.; Wang, Y.; Fu, M.; Lu, X. Recycled aggregate mortar enhanced by microbial calcite precipitation. *Mag. Concr. Res.* **2020**, *72*, 622–633. [CrossRef]
11. Kazmi, S.M.S.; Munir, M.J.; Wu, Y.-F.; Patnaikuni, I.; Zhou, Y.; Xing, F. Influence of different treatment methods on the mechanical behavior of recycled aggregate concrete: A comparative study. *Cem. Concr. Compos.* **2019**, *104*, 103398. [CrossRef]
12. Kim, Y.; Hanif, A.; Kazmi, S.M.S.; Munir, M.J.; Park, C. Properties enhancement of recycled aggregate concrete through pretreatment of coarse aggregates–Comparative assessment of assorted techniques. *J. Clean. Prod.* **2018**, *191*, 339–349. [CrossRef]
13. Rakul, B.R.; Olivia, M.; Won-Hee, K. Mechanical properties of steel fiber reinforced recycled aggregate concrete. *Struct. Concr.* **2018**, *20*, 745–755.
14. Kachouh, N.; El-Hassan, H.; El-Maaddawy, T. Effect of steel fibers on the performance of concrete made with recycled concrete aggregates and dune sand. *Constr. Build. Mater.* **2019**, *213*, 348–359. [CrossRef]
15. Gao, Y.; Wang, B.; Liu, C.; Hui, D.; Xu, Q.; Zhao, Q.; Hong, X. Experimental study on basic mechanical properties of recycled steel fiber reinforced concrete. *Rev. Adv. Mater. Sci.* **2022**, *61*, 417–429. [CrossRef]
16. Dong, J.F.; Wang, Q.Y.; Guan, Z.W. Material properties of basalt fibre reinforced concrete made with recycled earthquake waste. *Constr. Build. Mater.* **2017**, *130*, 241–251. [CrossRef]
17. Alnahhal, W.; Aljidda, O. Flexural behavior of basalt fiber reinforced concrete beams with recycled concrete coarse aggregates. *Constr. Build. Mater.* **2018**, *169*, 165–178. [CrossRef]
18. Mahmoud, N.; Alireza, A.; Amir, D.; Deihimi, A. Experimental study and modeling of fiber volume effects on frost resistance of fiber reinforced concrete. *Int. J. Civ. Eng.* **2018**, *16*, 263–272.
19. YaMei, Z.; ShenXia, C.; Bo, C.; Wei, S. Dry Shrinkage, Frost Resistance and Permeability of Rubber Included Concrete. *Key Eng. Mater.* **2006**, *302–303*, 120–124.
20. Limbachiya, M.C.; Leelawat, T.; Dhir, R.K. Use of recycled concrete aggregate in high-strength concrete. *Mater. Struct.* **2000**, *33*, 574–580. [CrossRef]
21. Deakins, D.; Bensemann, J.O. Achieving Innovation in a Lean Environment: How Innovative Small Firms Overcome Resource Constraints. *Int. J. Innov. Manag.* **2019**, *23*, 1950037. [CrossRef]
22. Hansen, T.C. Recycled aggregates and recycled aggregate concrete second state of the art report developments from 1945–1985. *Mater. Struct.* **1986**, *111*, 201–246. [CrossRef]
23. Jin, R.; Li, B.; Zhou, T.; Wanatowski, D.; Piroozfar, P. An empirical study of perceptions towards construction and demolition waste recycling and reuse in China. *Resour. Conserv. Recycl.* **2017**, *126*, 86–98. [CrossRef]
24. Júnior, N.S.A.; Silva, G.A.O.; Dias, C.M.R.; Ribeiro, D.V. Concrete containing recycled aggregates: Estimated lifetime using chloride migration test. *Constr. Build. Mater.* **2019**, *222*, 108–118. [CrossRef]
25. Meneses, E.J.; Gaussens, M.; Jakobsen, C.; Mikkelsen, P.S.; Grum, M.; Vezzaro, L. Coordinating rule-based and system-wide model predictive control strategies to reduce storage expansion of combined urban drainage systems: The case study of Lundtofte, Denmark. *Water* **2018**, *10*, 76. [CrossRef]
26. Cabral, A.E.B.; Schalch, V.; Molin, D.C.C.D.; Ribeiro, J.L.D. Mechanical properties modeling of recycled aggregate concrete. *Constr. Build. Mater.* **2010**, *24*, 421–430. [CrossRef]
27. Grilli, A.; Bocci, M.; Tarantino, A.M. Experimental investigation on fibre-reinforced cement-treated materials using reclaimed asphalt. *Constr. Build. Mater.* **2013**, *38*, 491–496. [CrossRef]
28. Peng, Z.; Shi, C.; Shi, Z.; Lu, B.; Wan, S.; Zhang, Z.; Chang, J.; Zhang, T. Alkali-aggregate reaction in recycled aggregate concrete. *J. Clean. Prod.* **2020**, *255*, 120238. [CrossRef]
29. Omary, S.; Ghorbel, E.; Wardeh, G. Relationships between recycled concrete aggregates characteristics and recycled aggregates concretes properties. *Constr. Build. Mater.* **2016**, *108*, 163–174. [CrossRef]
30. Bogas, J.A.; de Brito, J.; Ramos, D. Freeze-thaw resistance of concrete produced with fine recycled concrete aggregates. *J. Clean. Prod.* **2016**, *115*, 294–306. [CrossRef]
31. Richardson, A.; Coventry, K.; Bacon, J. Freeze/thaw durability of concrete with recycled demolition aggregate compared to virgin aggregate concrete. *J. Clean. Prod.* **2011**, *19*, 272–277. [CrossRef]
32. Topçu, I.B.; Şengel, S. Properties of concretes produced with waste concrete aggregate. *Cem. Concr. Res.* **2004**, *34*, 1307–1312. [CrossRef]
33. Tuyan, M.; Mardani-Aghabaglou, A.; Ramyar, K. Freeze-thaw resistance, mechanical and transport properties of self-consolidating concrete incorporating coarse recycled concrete aggregate. *Mater. Des.* **2014**, *53*, 983–991. [CrossRef]

34. Danying, G.; Lijuan, Z.; Jun, Z.; Peibo, Y. Durability of steel fibre-reinforced recycled coarse aggregate concrete. *Constr. Build. Mater.* **2020**, *232*, 117119.
35. Shengai, C.; Pin, L.; Enqi, C.; Jiao, S.; Bo, H. Experimental study on mechanical property and pore structure of concrete for shotcrete use in a hot-dry environment of high geothermal tunnels. *Constr. Build. Mater.* **2018**, *173*, 124–135.
36. Jinjie, H.; Yingze, J.; Qiang, Z. The influence of steel fiber-basalt fiber hybrid on the frost resistance of recycled concrete. *N. Build. Mater.* **2021**, *48*, 55–58. (In Chinese)
37. Mehran, K.; Mingli, G.; Majid, A. Effect of basalt fibers on mechanical properties of calcium carbonate whisker-steel fiber reinforced concrete. *Constr. Build. Mater.* **2018**, *192*, 742–753.
38. Min, H.; Yuru, Z.; Haonan, W.; Shihao, L. Mechanical Properties Test and Strength Prediction on Basalt Fiber Reinforced Recycled Concrete. *Adv. Civ. Eng.* **2021**, *2021*, 6673416.
39. John, B.; Sreekanta, D.; Sara, Y.K. Mechanical behaviour of basalt fibre reinforced concrete. *Constr. Build. Mater.* **2016**, *124*, 878–886.
40. Hao, Z.; Bin, J.; Hui, H.; Yanling, M. Experimental Study on Basic Mechanical Properties of Basalt Fiber Reinforced Concrete. *Materials* **2020**, *13*, 1362.
41. Chunsheng, Z.; Yanzhi, W.; Xianggang, Z.; Congzhi, G.; Kai, Z. Mechanical properties and microstructure of basalt fiber-reinforced recycled concrete. *J. Clean. Prod.* **2021**, *278*, 123252.
42. Chunsheng, Z.; Lei, W.; Xianggang, Z.; Yahong, D. A 3-dimensional prediction model for mechanical strength of basalt-steel fiber-reinforced recycled aggregate concrete based on reaction surface method. *Constr. Build. Mater.* **2021**, *303*, 124376.

Disclaimer/Publisher's Note: The statements, opinions and data contained in all publications are solely those of the individual author(s) and contributor(s) and not of MDPI and/or the editor(s). MDPI and/or the editor(s) disclaim responsibility for any injury to people or property resulting from any ideas, methods, instructions or products referred to in the content.